

Cluster simulation of relativistic fermions in two space-time dimensions

Uli Wolff*

Institut für Physik, Humboldt Universität
Newtonstr. 15
12489 Berlin, Germany

Abstract

For Majorana-Wilson lattice fermions in two dimensions we derive a dimer representation. This is equivalent to Gattringer's loop representation, but is made exact here on the torus. A subsequent dual mapping leads to yet another representation in which a highly efficient Swendsen-Wang type cluster algorithm is constructed. It includes the possibility of fluctuating boundary conditions. It also allows for improved estimators and makes interesting new observables accessible to Monte Carlo. The algorithm is compatible with the Gross-Neveu as well as an additional $Z(2)$ gauge interaction. In this article numerical demonstrations are reported for critical free fermions.

HU-EP-07/25

SFB/CCP-07-38

*e-mail: uwolff@physik.hu-berlin.de

1 Introduction

Occasionally in talks or papers about dynamical fermions it is mentioned — more or less as a joke — that the computer has no data-type Grassmann and one hence can simulate fermions only via the nonlocal effective theory after integrating them into the determinant. Of course, this is plagued by the well-known inefficiencies. In this article, based on Gattringer’s loop representation [1], we show that in two space-time dimensions one actually can get pretty close to ‘simulating Grassmann numbers’¹. We here expand on [1] and its recent numerical implementation [2] in several ways. First the loop representation is re-derived starting from Majorana fermions in what we think is a particularly natural way. The new connection includes definite boundary conditions on the torus and does not only work in the thermodynamic limit as before. In particular, we can then also approach the finite volume continuum limit. Furthermore we propose a cluster algorithm that is (practically) free of critical slowing down and allows for improved estimators. In this formulation we can simulate fluctuating boundary conditions which is necessary to allow for fixed (anti)periodic boundary conditions in the original fermion system. It also makes ratios of partition functions accessible as observables in Monte Carlo simulations. They constitute interesting quantities in the continuum limit.

The original Gross-Neveu model of self-coupled fermions in two dimensions [3] is most naturally written in terms of N species of Majorana fermions. In the lattice discretization with Wilson fermions the euclidean action is given by [4]

$$S = a^2 \sum_x \left\{ \frac{1}{2} \xi^\top \mathcal{C} (\gamma_\mu \tilde{\partial}_\mu + m - \frac{r}{2} a \partial^* \partial) \xi - \frac{g^2}{8} (\xi^\top \mathcal{C} \xi)^2 \right\}. \quad (1.1)$$

The Grassmann-valued field $\xi \equiv \xi_{\alpha i}(x)$ has a spin index $\alpha = 1, 2$ and a flavor index $i = 1, \dots, N$ that we leave implicit. We denote by $\partial, \partial^*, \tilde{\partial}$ the forward, backward and symmetric nearest neighbor differences on our cubic $T \times L$ lattice. The charge conjugation matrix \mathcal{C} obeys

$$\mathcal{C} \gamma_\mu \mathcal{C}^{-1} = -\gamma_\mu^\top = -\gamma_\mu^*, \quad \mathcal{C} = -\mathcal{C}^\top. \quad (1.2)$$

For even N each pair of Majorana fermions may be considered as one Dirac fermion

$$\psi = \frac{1}{\sqrt{2}} (\xi_1 + i \xi_2), \quad \bar{\psi} = \frac{1}{\sqrt{2}} (\xi_1^\top - i \xi_2^\top) \mathcal{C} \quad (1.3)$$

with its independent $\psi, \bar{\psi}$. In the Majorana form the full global symmetry group $O(N)$ is manifest beside (without Wilson term) the discrete γ_5 symmetry whose

¹Cum grano salis.

spontaneous breaking was studied in [3] in the $N \rightarrow \infty$ limit. The model is renormalizable in the strict sense: there is no other $O(N)$ invariant scalar 4-fermion interaction term. For $N = 2$ we have the Thirring model [5], [6], the cases $N \geq 3$ are expected to be asymptotically free. In the remainder of this paper we set the Wilson parameter to $r = 1$ and work in lattice units $a = 1$. The discrete chiral symmetry $\xi \rightarrow \gamma_5 \xi$ of the massless continuum theory is broken by the Wilson term and is only expected to be recovered in the continuum limit at the critical mass $m = m_c$. On the torus we consider four conceivable combinations of periodic or antiperiodic boundary conditions in the two directions. Periodicity angles different from $0, \pi$ — as sometimes used for Dirac fermions — would not lead to a periodic action density for Majorana fermions. We label the possible boundary conditions by a bit-vector

$$\varepsilon_\mu, \quad \varepsilon_0, \varepsilon_1 \in \{0, 1\} \quad (1.4)$$

where 0 stands for periodic and 1 for antiperiodic boundary conditions in the corresponding direction.

Often the interaction term is factorized by the introduction of an auxiliary bosonic field. For us it will be more convenient to think of $m \rightarrow m(x)$ as an x -dependent mass for a while. If $Z_\xi^\varepsilon[m]$ is the partition function of one free Majorana fermion with boundary condition ε_μ in this background field, then the partition function of the interacting theory is written as

$$Z_{\text{int}} = \exp \left\{ \frac{g^2}{2} \sum_x \frac{\partial^2}{\partial m(x)^2} \right\} (Z_\xi^\varepsilon[m])^N. \quad (1.5)$$

Integrating the fermions in the remaining Gaussian problem yields the Pfaffian

$$Z_\xi^\varepsilon[m] = \text{Pf} \left[\mathcal{C}(\gamma_\mu \tilde{\partial}_\mu + m - \frac{1}{2} \partial^* \partial) \right]. \quad (1.6)$$

In appendix A one can find a reminder of the definition of Pfaffians. For even N we may replace the Pfaffians by the $N/2$ power of the determinant. In this form and with a factorizing field, the model can be simulated by standard methods like HMC as carried out in [4]. For larger g this compute-intensive task became rather difficult due to singularities developing in the operator under the Pfaffian. Of course, the model itself remains completely well-defined on any finite lattice. Fermionic and compact bosonic variables are safe in this respect.

As a first step we now introduce the loop representation [1] of $Z_\xi^\varepsilon[m]$. It may in fact also be looked upon as a dimer ensemble similar to those derived in [7] for strong coupling QCD.

2 External field fermion partition function

As a building block for the Gross-Neveu models we consider for a single Majorana field the external field action

$$S = \frac{1}{2} \sum_x \varphi(x) \xi^\top(x) \mathcal{C} \xi(x) - \sum_{x,\mu} \tau(x,\mu) \xi^\top(x) \mathcal{C} P(\hat{\mu}) \xi(x + \hat{\mu}). \quad (2.1)$$

We assume a lattice with T sites in the time direction ($\mu = 0$) and L sites in the space direction ($\mu = 1$). The variables $\varphi(x) = 2 + m(x)$ and $\tau(x,\mu)$ are external commuting fields. The link field τ is introduced for completeness. It will be dropped at some point. The lattice derivatives in (1.1) combine to Wilson projectors that we define for arbitrary lattice unit vectors $n = \pm \hat{\mu}$

$$P(n) = \frac{1}{2}(1 - n_\mu \gamma_\mu), \quad (\mathcal{C}P(n))^\top = -\mathcal{C}P(-n). \quad (2.2)$$

The last identity implies

$$\xi^\top(x) \mathcal{C} P(\hat{\mu}) \xi(x + \hat{\mu}) = \xi^\top(x + \hat{\mu}) \mathcal{C} P(-\hat{\mu}) \xi(x). \quad (2.3)$$

While the field ξ has torus periodicity ε , the external fields φ, τ are continued periodically to obtain a periodic action density.

Defining the ‘covariant’ projecting hop operator

$$(H_\mu \xi)(x) = \tau(x,\mu) \mathcal{C} P(\hat{\mu}) \xi(x + \hat{\mu}) \quad (2.4)$$

we may, with the help of (2.3), also write the action in the manifestly antisymmetric short-hand form

$$S = \frac{1}{2} \sum_x \varphi \xi^\top \mathcal{C} \xi - \frac{1}{2} \sum_{x,\mu} \xi^\top (H_\mu - H_\mu^\top) \xi \quad (2.5)$$

where H_μ^\top is transposed with respect to both spin and space indices yielding

$$(H_\mu^\top \xi)(x) = -\tau(x - \hat{\mu}, \mu) \mathcal{C} P(-\hat{\mu}) \xi(x - \hat{\mu}). \quad (2.6)$$

Now we are ready for the partition function

$$Z_\xi^\varepsilon[\varphi, \tau] = \int D\xi e^{-S}. \quad (2.7)$$

The measure is

$$D\xi = \prod_x (d\xi_1 d\xi_2)(x) \quad (2.8)$$

and yields

$$Z_\xi[\varphi, \tau] = \text{Pf} \left(\varphi \mathcal{C} - \sum_{\mu} (H_{\mu} - H_{\mu}^{\top}) \right) \quad (2.9)$$

which is a nonlocal expression in the external fields as in the case of the usual Dirac fermion determinant. In appendix A we evaluate the Pfaffian for $\tau \equiv 1$ and constant φ for all four boundary conditions.

3 Equivalent statistical systems

3.1 Dimer representation

The Grassmannian Boltzmann factor may be expanded,

$$Z_\xi = \int D\xi \prod_x \{1 + \varphi \xi_2 \xi_1\} \prod_{x,\mu} (1 + \tau(x, \mu) \xi^{\top}(x) \mathcal{C} P(\hat{\mu}) \xi(x + \hat{\mu})). \quad (3.1)$$

All fields in the curly bracket are at x and this factor is best considered as part of the measure. We have here chosen \mathcal{C} such that $\frac{1}{2} \xi^{\top} \mathcal{C} \xi = \xi_1 \xi_2$ which just amounts to a phase convention. Note that the square of the hop-term vanishes due to the one-dimensional projectors. There is only one linear combination of the two Grassmann numbers contributing from each site which squares to zero. We now introduce one-bit-valued dimer or bond variables [7] on each link $k(x, \mu) = 0, 1$, whose values are used to organize the expansion as

$$Z_\xi[\varphi, \tau] = \sum_{\{k(x,\mu)\}} \int D\xi \prod_x \{1 + \varphi \xi_2 \xi_1\} \prod_{x,\mu} (\tau(x, \mu) \xi^{\top}(x) \mathcal{C} P(\hat{\mu}) \xi(x + \hat{\mu}))^{k(x,\mu)}. \quad (3.2)$$

As in [7] the goal now is to integrate out the fermions to yield a Boltzmann weight $\rho[k]$ for each dimer configuration. By asking how the Grassmann integrations can be saturated site by site it is clear that a non-zero weight only arises if at each site there are either two dimers adjacent from different links or none at all. In the latter case the integration is saturated by the measure term and a factor $\varphi(x)$ appears for this site. We also call these contributions monomers. Due to the above constraint the dimers have to form closed non-intersecting and non-backtracking loops. We choose randomly a starting point and an orientation on such a loop such that along the loop one visits the sites (x_1, x_2, \dots, x_l) . Consecutive sites differ by lattice unit vectors, $x_{i+1} = x_i + \hat{n}_i$, including $x_1 = x_l + \hat{n}_l$ in the last step. For such a loop the product of bilinears

$$(\xi^{\top}(x_1) \mathcal{C} P(\hat{n}_1) \xi(x_2)) (\xi^{\top}(x_2) \mathcal{C} P(\hat{n}_2) \xi(x_3)) \cdots (\xi^{\top}(x_l) \mathcal{C} P(\hat{n}_l) \xi(x_1)) \quad (3.3)$$

has to be considered together with the integrations on the l sites involved. Note that here (2.3) is relevant on the links that are transversed in the negative direction. The trivial key formula is, for a single site,

$$\int d\xi_1 d\xi_2 \xi \xi^\top = \mathcal{C}^{-1}. \quad (3.4)$$

Now the expression (3.3) integrates to

$$X = -\text{tr}[P(\hat{n}_1)P(\hat{n}_2)\cdots P(\hat{n}_l)]. \quad (3.5)$$

Here appears the very important minus sign for a closed fermion loop, well-known for instance from Feynman diagrams. It is not difficult to see that this result is independent of the starting point and orientation chosen.

The evaluation of the spin factor follows [8]. Let us introduce eigenspinors of the projectors

$$P(\hat{n}_i) = |\hat{n}_i\rangle \langle \hat{n}_i|, \quad \langle \hat{n}_i | \hat{n}_i \rangle = 1, \quad (3.6)$$

$$X = -\langle \hat{n}_1 | \hat{n}_2 \rangle \langle \hat{n}_2 | \hat{n}_3 \rangle \cdots \langle \hat{n}_l | \hat{n}_1 \rangle \quad (3.7)$$

A spinor is rotated by an angle θ by the unitary spin matrix $R(\theta) = \exp[(\theta/2)\gamma_0\gamma_1]$. This allows us to write

$$|\hat{n}_i\rangle = R(\Delta\theta_i)|\hat{n}_{i+1}\rangle \quad \Delta\theta_i \in \{0, \pm\pi/2\}, \quad i = 1, 2, \dots, l \quad (3.8)$$

with $\hat{n}_{l+1} = \hat{n}_1$. Using

$$\langle \hat{n}_j | R(\Delta\theta_i) | \hat{n}_j \rangle = \cos(\Delta\theta_i/2) \quad (3.9)$$

we get to

$$X = -\langle \hat{n}_l | \hat{n}_1 \rangle \prod_{i=1}^{l-1} \cos(\Delta\theta_i/2). \quad (3.10)$$

The rotation accumulated in steps (3.8) is

$$|\hat{n}_1\rangle = R(\Theta - \Delta\theta_l)|\hat{n}_l\rangle \quad \text{with} \quad \Theta = \sum_{i=1}^l \Delta\theta_i. \quad (3.11)$$

For closed paths we have $\Theta = 2\pi\nu$ and $R(\Theta - \Delta\theta_l) = \cos(\pi\nu)R(-\Delta\theta_l)$. For the nonzero lattice angles, $\cos(\Delta\theta_i/2) = 1/\sqrt{2}$. Altogether the final result is

$$X = (-)^{\nu+1} 2^{-N_c/2}, \quad (3.12)$$

where N_c is the number of $\pm\pi/2$ angles ('corners') occurring along the loop and $\nu = 0, \pm 1$ is the number of complete rotations the loop makes. The extra minus

sign for $|\nu| = 1$ is the one associated with fermions under 2π -rotations. If we include a non-trivial τ field then the product of its Wilson loops for all dimer loops appear in addition in the weight. After this remark we set $\tau \equiv 1$ until further notice.

Although we are on a lattice here, we can define homotopy classes of loops. Two loops are homotopic to each other if they can be transformed into each other by a sequence of steps, where dimers are only changed around a single plaquette. We see from the above that X is positive for all configurations containing only loops that are homotopic to the trivial loop, just a point. The two minus signs characteristic of fermions compensate each other in this class!

Loops can wind however around the torus in either direction as noted in [2]. A pair of loops winding around the same direction is still in the trivial homotopy class. An odd number of windings leads however to a new class. This may also happen in both directions at the same time and hence there are the four classes $\mathcal{L}_{00}, \mathcal{L}_{10}, \mathcal{L}_{01}, \mathcal{L}_{11}$. In figure 1 we show a representative of each class. They are equilibrium configurations of free fermions at $m = 0$ and $T = L = 10$. The meaning of the $+/-$ signs in the plots will become clear later. Only configurations from \mathcal{L}_{00} have a positive weight while in the other cases there is an odd number of closed loops with zero total rotation angle each of which contributes a factor -1 . By introducing *antiperiodic* boundary conditions in some direction the loops closing around that direction receive yet another sign without changing the topologically trivial ones.

With the local weight

$$\rho[k] = \prod_x f(k, x) \quad (3.13)$$

with

$$f(k, x) = \begin{cases} \varphi(x) & \text{if monomer at } x \\ 1 & \text{if 2 dimers in the same direction at } x \\ 1/\sqrt{2} & \text{if 2 dimers in different directions at } x \\ 0 & \text{else} \end{cases} \quad (3.14)$$

we now define the positive dimer partition functions

$$Z_k^{00}[\varphi] = \sum_{\{k(x,\mu)\} \in \mathcal{L}_{00}} \rho[k], \quad Z_k^{10}(\varphi) = \sum_{\{k(x,\mu)\} \in \mathcal{L}_{10}} \rho[k], \quad \text{etc.} \quad (3.15)$$

From what was said above the connections

$$4Z_k^{00}[\varphi] = +Z_\xi^{00}[\varphi] + Z_\xi^{10}[\varphi] + Z_\xi^{01}[\varphi] + Z_\xi^{11}[\varphi] \quad (3.16)$$

$$4Z_k^{10}[\varphi] = -Z_\xi^{00}[\varphi] + Z_\xi^{10}[\varphi] - Z_\xi^{01}[\varphi] + Z_\xi^{11}[\varphi] \quad (3.17)$$

$$4Z_k^{01}[\varphi] = -Z_\xi^{00}[\varphi] - Z_\xi^{10}[\varphi] + Z_\xi^{01}[\varphi] + Z_\xi^{11}[\varphi] \quad (3.18)$$

$$4Z_k^{11}[\varphi] = -Z_\xi^{00}[\varphi] + Z_\xi^{10}[\varphi] + Z_\xi^{01}[\varphi] - Z_\xi^{11}[\varphi] \quad (3.19)$$

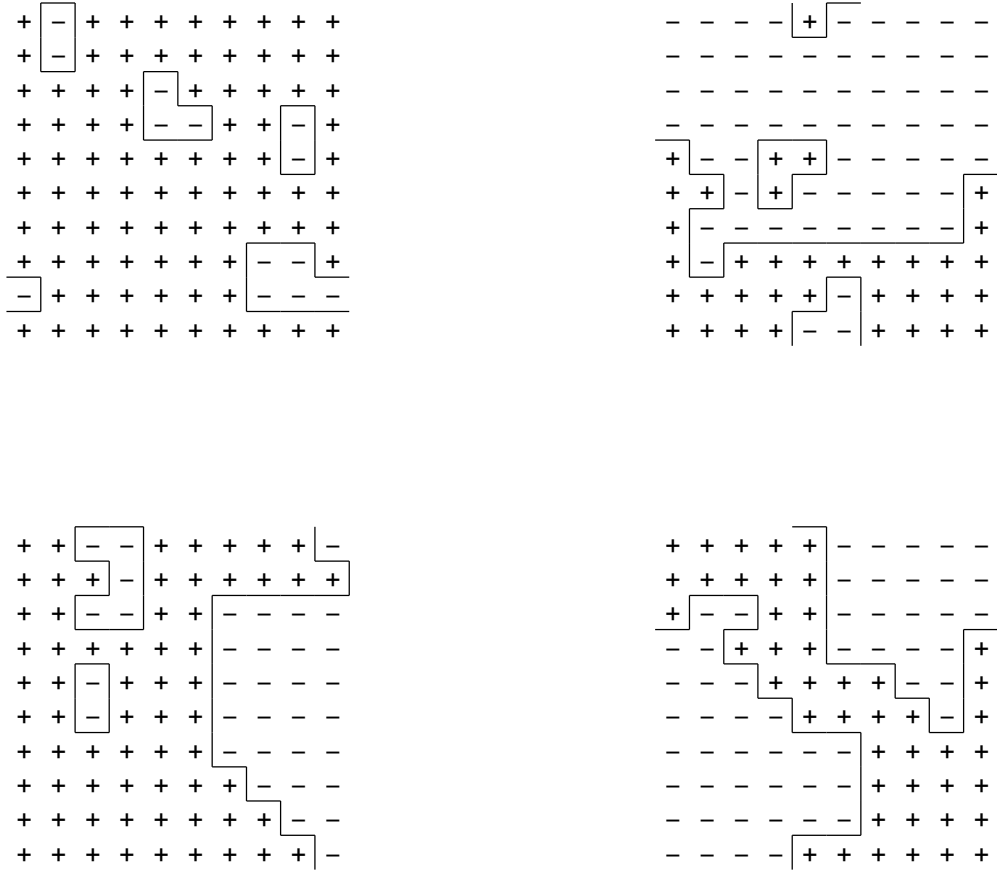


Figure 1: Examples of dimer configurations (solid lines) in the topological classes $\mathcal{L}_{00}, \mathcal{L}_{10}, \mathcal{L}_{01}, \mathcal{L}_{11}$ (from upper left to lower right). The time direction ($\mu = 0$) points to the right. The signs refer to spins on the dual lattice.

arise, which can be inverted. If we want to realize the boundary conditions $\epsilon_\mu = (1, 0)$ of [4] (or actually any other definite choice for the fermions) we have to sum over all dimer classes including negative weight contributions

$$Z_\xi^{10}[\varphi] = Z_k^{00}[\varphi] + Z_k^{10}[\varphi] - Z_k^{01}[\varphi] + Z_k^{11}[\varphi]. \quad (3.20)$$

All these relations between partition functions can be turned into relations between expectation values of the scalar fermion density and monomer densities by differentiating with respect to $\varphi(x)$. One example based on (3.20) is

$$-\frac{\varphi(x)}{2} \langle \xi^\top(x) \mathcal{C} \xi(x) \rangle_{10} = \frac{Z_k^{00} \langle K(x) \rangle_{00} + Z_k^{10} \langle K(x) \rangle_{10} - Z_k^{01} \langle K(x) \rangle_{01} + Z_k^{11} \langle K(x) \rangle_{11}}{Z_k^{00} + Z_k^{10} - Z_k^{01} + Z_k^{11}}. \quad (3.21)$$

The observable $K(x)$ is one if there is a monomer at x and zero otherwise. With the help of $\tau(x, \mu)$ as a source one could establish further relations.

For free fermions ($\varphi = 2 + m$) in the thermodynamic limit at fixed $m > 0$ the various Z_ξ^ϵ differ only by exponentially small amounts and Z_k^{00} dominates among the dimer ensembles. Taking the finite volume continuum limit ($L \rightarrow \infty$ with Lm fixed, see appendix A) and in particular for $m = 0$ this is not so. In the latter case we have an exact zero fermion mode for $\epsilon_\mu = (0, 0)$ and $Z_\xi^{00} = 0$ holds. This implies

$$Z_k^{00} = Z_k^{10} + Z_k^{01} + Z_k^{11} \quad \text{for } m = 0. \quad (3.22)$$

3.2 Spin representation

In this subsection we transform the dimer system to yet another representation by Ising spins. This will allow us to design a global cluster algorithm. A clue that this may be possible is given by the idea that a natural way to manage and modify the closed loops in the dimer formulation is to consider them as boundaries of domains of up-spins surrounded by down-spins (Peierls contours).

The spins that we introduce live on the lattice dual to the one carrying the fermionic and the dimer variables. Its sites labelled by underlined \underline{x} are dual to plaquettes of the original lattice and are imagined to be located at their centers. Analogously, the sites of the original lattice are dual to plaquettes in the new one. Links (x, μ) and $(\underline{x}, \underline{\mu})$ are dual to each other if they cross, see figure 2. The idea is now to put an Ising field $s(\underline{x})$ on the dual lattice and to identify configurations

$$k(x, \mu) = \begin{cases} 1 & \text{if } s(\underline{x})s(\underline{x} + \widehat{\underline{\mu}}) = -1 \\ 0 & \text{if } s(\underline{x})s(\underline{x} + \widehat{\underline{\mu}}) = +1 \end{cases} . \quad (3.23)$$

In other words, dimers are located where nearest neighbor spins on the dual lattice are antiparallel. In a first stage we restrict ourselves to the class \mathcal{L}_{00} of dimer configurations.

We first prove that for each admissible dimer configuration there are exactly two spin fields obeying (3.23) that differ by a global spin-flip. In a first step we define a $Z(2)$ lattice gauge field² on the dual lattice in terms of the dimers on the original lattice

$$\sigma(\underline{x}, \underline{\mu}) = \begin{cases} +1 & \text{if } k(x, \mu) = 0 \\ -1 & \text{if } k(x, \mu) = 1 \end{cases} . \quad (3.24)$$

Because of the constraints on k this gauge field is unity when multiplied around any plaquette (on the dual lattice). As we restrict ourselves to \mathcal{L}_{00} here, also loops around the torus are unity for this gauge field. Thus σ is a pure gauge on the

²This field has nothing to do with the earlier τ .

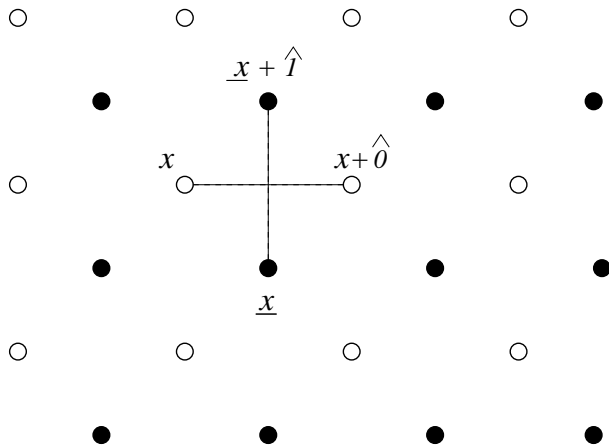


Figure 2: Illustration of the labelling of the original and the dual lattice.

torus with a periodic gauge function. The spin-field is this gauge function that we construct now. We choose a site \underline{y} (the origin, for example) and set $s(\underline{y}) = +1$. Now this value is parallel-transported with σ to all other sites, for instance along a maximal tree rooted at \underline{y} . Due to the absence of curvature in σ , the result is path-independent, consistent and unique. Starting from $s(\underline{y}) = -1$ we obtain the other configuration associated with $\{k(x, \mu)\}$. The signs in figure 1 are just these spins.

While we now have exactly two spin fields for each admissible dimer configuration in \mathcal{L}_{00} , not all conceivable spin fields are reached in this way. Obviously, spin configurations, that on any plaquette look like

$$\begin{pmatrix} s_4 & s_3 \\ s_1 & s_2 \end{pmatrix} = \begin{pmatrix} - & + \\ + & - \end{pmatrix}, \begin{pmatrix} + & - \\ - & + \end{pmatrix} \quad (3.25)$$

do not occur in the image, where we here just gave simple labels to the four spins. They would correspond to crossing loops not allowed by the original Grassmann variables. If this is however excluded on all plaquettes, then we can reconstruct admissible $\{k(x, \mu)\}$ configurations from $\{s(\underline{x})\}$. The total Boltzmann factor in the spin representation is now a big product with one factor for each plaquette. These weights w are given in table 1 which lists only 8 of the 16 configurations and is completed by using $w(s_1, s_2, s_3, s_4) = w(-s_1, -s_2, -s_3, -s_4)$. The monomer strength $\varphi(x)$ is taken here at the site x of the original lattice sitting at the center of the dual plaquette considered.

The derivation of this representation resembles the construction of the dual formulation for generalized Ising models [9]. We summarize it (giving the ordinary self-dual two-dimensional Ising model as an example in brackets): One first introduces new variables living on the bonds making up the Hamiltonian of the

s_1	s_2	s_3	s_4	w
+	+	+	+	$\varphi(x)$
+	+	+	-	$1/\sqrt{2}$
+	+	-	+	$1/\sqrt{2}$
+	-	+	+	$1/\sqrt{2}$
-	+	+	+	$1/\sqrt{2}$
+	+	-	-	1
+	-	-	+	1
+	-	+	-	0

Table 1: Plaquette weights depending on the spin configuration.

original theory (a link field). Then the original spins are summed over producing a constraint in the new variables (vanishing plaquettes of the links interpreted on the dual lattice). This constraint is then solved on the dual lattice (links given as a pure gauge by a site field). The extension of the concept here is that we change from Grassmann elements to bosonic variables, have an additional constraint (3.25) to fulfill, and that there can be minus signs. One could talk of Fermi-Bose- or super-duality.

The plaquette weight can also be written in terms of pairwise nearest neighbor bond-interactions of the form [writing $\delta_{ij} \equiv \delta_{s_i s_j} \equiv \frac{1}{2}(1 + s_i s_j)$]

$$w(s_1, s_2, s_3, s_4) = \{p[\delta_{12} + \delta_{23} + \delta_{34} + \delta_{41}] + q[\delta_{12}\delta_{34} + \delta_{14}\delta_{23}] + r[\delta_{12}\delta_{14} + \delta_{21}\delta_{23} + \delta_{32}\delta_{34} + \delta_{41}\delta_{43}]\}, \quad (3.26)$$

with the x -dependence in p, q, r suppressed. To match table 1, the following equations have to hold

$$\begin{aligned} \varphi(x) &= 4p + 2q + 4r \\ \frac{1}{\sqrt{2}} &= 2p + r \\ 1 &= 2p + q. \end{aligned}$$

The solution of this system is

$$r = \frac{1}{4}(\varphi - 2) = \frac{m}{4}, \quad p = \frac{1}{2\sqrt{2}} - \frac{r}{2}, \quad q = 1 - \frac{1}{\sqrt{2}} + r. \quad (3.27)$$

We remark here that all coefficients are positive for $0 \leq m \leq 2\sqrt{2} \approx 2.83$. In the free case, this clearly covers the relevant range of bare masses.

If we now include dimer configurations in the other sectors by using (3.23), the only difference is that the resulting $s(x)$ is antiperiodic in the direction *orthogonal* to those where dimer loops run around the torus. Thus \mathcal{L}_{10} corresponds

to spin-fields antiperiodic in *space*, \mathcal{L}_{01} to those in *time* and \mathcal{L}_{11} to spins with both directions antiperiodic. The mechanism here is that antiperiodic boundary conditions of the spins force an interface into their configurations which leads to the nontrivial dimer loop topology. Introducing further partition functions Z_s for the spin ensembles we relate

$$Z_k^{00} = \frac{1}{2}Z_s^{00}, \quad Z_k^{10} = \frac{1}{2}Z_s^{01}, \quad Z_k^{01} = \frac{1}{2}Z_s^{10}, \quad Z_k^{11} = \frac{1}{2}Z_s^{11}. \quad (3.28)$$

The factor $1/2$ cancels the global spin-flip symmetry. Again, by differentiation, we may relate expectation values, where the presence (absence) of a monomer yielding $K(x) = 1(0)$ in the spin language translates into maximally ‘polarized’ plaquettes where all four spins are parallel,

$$K(x) = \delta_{4,|M(x)|}, \quad M(x) = \sum_{\underline{x} \text{ around } x} s(\underline{x}). \quad (3.29)$$

4 Simulation algorithms

4.1 Local algorithms

A local algorithm to simulate any one of the above dimer ensembles with all weights taken positive was recently described and tested by Gatttringer et al. [2]. The simplest case to consider is a free Majorana fermion of mass m with $\varphi(x) = 2 + m$. In the updates one actually performs only changes that are local in the homotopy-sense by proposing dimer-flips $k(x, \mu) \rightarrow 1 - k(x, \mu)$ around plaquettes. The move is accepted with the Metropolis probability corresponding to the ratio of ρ in (3.13) for the new and the old configuration, which is a locally computable quantity. Of course, it vanishes, if the new configuration would violate one of the constraints. This update stays in the homotopy class fixed by the starting configuration (see figure 1) and is ergodic within it. Thus the various ensembles can be simulated which correspond to combinations of periodic and antiperiodic Pfaffians. In [2] it was demonstrated that already such simulations are vastly more efficient than HMC type simulations.

The entirely equivalent update in the Ising form consists of local spin-flips. The Metropolis decision in this case depends on the eight nearest and next-to-nearest (diagonal) neighbors that share plaquettes with the spin in focus. The numerical efficiency in both forms is very similar.

4.2 Cluster algorithm

The plaquette interaction in (3.26) is now written as a superposition of 10 different terms, schematically given by

$$w(s_1, s_2, s_3, s_4) = \sum_{i=1}^{10} P_i \Delta_i(s_1, s_2, s_3, s_4) \quad (4.1)$$

with $P_i \in \{p, q, r\}$ and $\Delta(s_1, s_2, s_3, s_4) \in \{0, 1\}$. In complete analogy to [10] we introduce now ten-valued bond variables $b(x)$ with each value corresponding to one of these terms to obtain

$$Z_s = \sum_{\{b(x), s(\underline{x})\} \text{ plaq}} \prod P_{b(x)} \Delta_{b(x)}(s_1, s_2, s_3, s_4). \quad (4.2)$$

To avoid a too clumsy notation here again s_1, s_2, s_3, s_4 are spins around each of the plaquettes. The celebrated trick of [10] consists of Monte Carlo sampling *both* the b and the s variables. As the first part of an update cycle one chooses new b at fixed s by a local heatbath procedure. Of course, in general, the choice is between less than 10 possibilities, as some of the $\Delta_{b(x)}(s_1, s_2, s_3, s_4)$ vanish. Then, for given bonds b , any of the 2^{TL} spin configurations has either weight zero or a constant nonzero weight depending on the constraints given by the product of all factors $\Delta_{b(x)}$. Just as in the standard Ising model case we now construct the percolation clusters defined by the active bonds in all $\{\Delta_{b(x)}\}$. By flipping the spins in each cluster as a whole with probability 1/2, we sample one of the allowed and equally weighted spin configurations. The overall procedure amounts to a global independent sampling of spins (at fixed bonds) and will be numerically demonstrated to almost eliminate critical slowing in section 5.

At the stage of selecting a new spin field one may also construct improved cluster estimators. This is achieved, if, for some observable, one is able to analytically average over all conceivable spin-assignments of which only one is taken as the next configuration.

While the above procedure is analogous to the well-known Swendsen-Wang algorithm [10] we could also study a single cluster variant [11]: one spin is chosen at random, and then only the one cluster connected to it is constructed by investigating the plaquette terms touched in the growth process until it stops. Then spins on this cluster are always flipped. This may well be even more efficient as large clusters are preferred.

We end this subsection with a remark on the global spin flip symmetry. At first one may think that it is a (slightly) annoying redundancy in the new representation. However, it is in fact essential to be able to grow clusters whose energy (action) is associated with the surface (in our case the loops) and not with the

bulk. Loosely speaking, as one grows a (single) cluster, there is always an energetic ‘way out’ by flipping the whole lattice. Of course, if this is all that happens, that algorithm will not be efficient. The auxiliary percolation problem allows to find nontrivial clusters.

4.3 Fluctuating boundary conditions

In (3.20) we saw that it is desirable to also be able to simulate enlarged ensembles where one sums beside configurations of spins also over several possible boundary conditions. If in conventional simulations one proposes a change of the boundary conditions at fixed spins, one generates energy (action) proportional to T or L and the proposal will practically always be rejected. It was noticed however in [12] that with cluster algorithms the situation can be different. In the step where we pick new spins at fixed bonds the search among possible equally weighted new configurations can be enlarged to also include changed boundary conditions. If we label them by ε_μ again (for the spins now) the four possible ε become a dynamical variable. In [12] these changes were introduced in a single-cluster/Metropolis spirit, which would also be possible — in fact less involved — here. In view of the future construction of improved estimators we stick however to the many-cluster view and design now a correspondingly generalized cluster algorithm. It consists of the following steps:

- We throw bonds on the links as discussed before.
- We determine by some percolation algorithm (e.g. tree search) the independent spin clusters connected by bonds *but ignore* two layers of links such that the torus is cut open. We take $\{(x, 0)|_{x_0=T-1}\}$ and $\{(x, 1)|_{x_1=L-1}\}$. We call these clusters preclusters, their connectivity is determined in the ‘interior’. Each of them carries a unique cluster label as a result.
- Now the remaining links are examined as far as they have been activated. We call these bonds clamps. They have the effect of sewing up (some of) the preclusters. This is done by the pointer technique described in [13]. We may visualize the process as a graph with the preclusters as blobs, some of which get connected by lines.
- In this process à la [13] one can detect when closed loops in the graph are formed. We set one of four types of flags whenever a loop is closed. They distinguish whether an odd or an even number of temporal or spatial clamps are met around the loop. We end with flags $f_{00}, f_{10}, f_{01}, f_{11}$ each being zero or one.

- Boundary conditions ε are only compatible with this loop structure if for all occurring loops with flag up ($f_{\alpha\beta} = 1$) the condition $\alpha\varepsilon_0 + \beta\varepsilon_1 = 0 \pmod{2}$ holds. Of course, $\varepsilon = (0, 0)$ is always allowed.
- Among the compatible ε (1,2 or 4 values) one is chosen with equal probability.
- Now flips for all preclusters are determined and executed. Connected components of the graph flip together, but preclusters within these components can flip relative to each other if the boundary condition has changed. The above construction guarantees that the orientations thus propagated do not depend on the path that is taken on the graph.

Although rather short and compact in the end this is not a trivial code to write. It is helpful to organize it under a geometric point of view focussing on parallel transport between preclusters with a $Z(2)$ group, where the boundary conditions are gauge variables on the clamps. Of course, as we can solve the free fermion ensembles exactly (appendix A) and easily get high accuracy with cluster simulations, many significant checks by short simulations (taking seconds) were available. A very good monitor for debugging at every stage is to set traps for the occurrence of illegal plaquettes (3.25). An alternative strategy to move boundary conditions would be to turn the loop structure of the above graph into a system of linear equations in the Galois field of two elements (addition isomorphic to logical `xor`). Following [14] and [15] this can be solved by Gauss elimination.

The above scheme contains some nested pointer operations. One could be worried in principle whether the execution time grows more than linearly with the lattice volume. In practice there was found to be absolutely no problem of this kind. This is in fact the same for cluster simulations of the standard Ising model using the algorithm of [13]. In our case the problem is even less severe as the number of clamps is smaller than $T + L$, not proportional to the volume.

4.4 Negative mass

For free fermions one could content oneself with the parameter range $m \geq 0 = m_c$. On the other hand all results in appendix A can be taken at arbitrary m . After all, the partition function on the finite lattice is just a polynomial. When we later come back to the interacting theory, it will also turn out, that negative mass fermions will be required because $m_c < 0$ due to renormalization. The local algorithm [2] works for negative m , a sign problem only arises if $\varphi = 2 + m$ changes sign. The bond probabilities (3.27) however restrict the cluster algorithm so far to $m \geq 0$. Luckily, there is an alternative decomposition of the plaquette interaction into bonds that comes to rescue when $m(x)$ is negative.

The r -term in (3.26) is replaced by

$$\frac{\tilde{r}}{2}[\delta_{12}\bar{\delta}_{14} + \delta_{21}\bar{\delta}_{23} + \delta_{32}\bar{\delta}_{34} + \delta_{41}\bar{\delta}_{43} + \bar{\delta}_{12}\delta_{14} + \bar{\delta}_{21}\delta_{23} + \bar{\delta}_{32}\delta_{34} + \bar{\delta}_{41}\delta_{43}],$$

where we introduced also antibonds $\bar{\delta}_{ij} \equiv 1 - \delta_{ij}$. The two other terms are unchanged but the coefficients are now \tilde{p}, \tilde{q} . Using $\delta_{12}\bar{\delta}_{14} = \delta_{12} - \delta_{12}\delta_{14}$ etc. one sees that the new weight coincides with the old one if we identify $r = -\tilde{r}$ and $p = \tilde{p} + \tilde{r}$. The matching equations are now

$$\begin{aligned}\varphi(x) &= 4\tilde{p} + 2\tilde{q} \\ \frac{1}{\sqrt{2}} &= 2\tilde{p} + \tilde{r} \\ 1 &= 2\tilde{p} + \tilde{q} + 2\tilde{r},\end{aligned}$$

solved by

$$\tilde{r} = \frac{1}{4}(2 - \varphi) = \frac{-m}{4}, \quad \tilde{p} = \frac{1}{2\sqrt{2}} - \frac{\tilde{r}}{2}, \quad \tilde{q} = 1 - \frac{1}{\sqrt{2}} - \tilde{r}. \quad (4.3)$$

Now all weights are positive for $-m \leq 2(2 - \sqrt{2}) \approx 1.17$.

The presence of antibonds is compatible with the cluster search including fluctuating boundary conditions. With an $m(x)$ that changes sign over one lattice, one actually decomposes some plaquettes with (3.27) and others with (4.3). One must however not make the mistake to think of the preclusters as ferromagnetic (Weiss) domains, they contain in general both up and down spins. This is why we took care to talk about distributing flips to clusters rather than assigning new spin orientations to them as whole.

5 Numerical applications

We now report on numerical experiments. In this first publication on the method we stick to free fermions and the observable $K(x)$. It corresponds to the scalar fermion density and is mainly used to diagnose the algorithm. Hence, with the results of appendix A, every computed mean value is known exactly and was verified to be reproduced by the Monte Carlo simulations within errors. We do not plot results for K . They are too boring: errors not visible on the graph and exact results agreeing with the data within 1 and occasionally up to around 2 sigma.

For the algorithm, the non-interacting case does not seem to be fundamentally different from the interacting Gross-Neveu model. All details necessary for this extension are given, but the numerical implementation is deferred to a future investigation. What remains to be seen is how the correlation between monomers of different flavor influences the Monte Carlo dynamics at stronger coupling.

5.1 Critical slowing

We performed a series of simulations of one species of free Majorana fermions at the critical value $m = 0$. In this case, the only infrared scale is given by the system size $T = L = 8 \dots 128$. We simulated the trivial ensembles corresponding to the loop class \mathcal{L}_{00} . Results are summarized in table 2. Each run with the local algorithm, passing through the lattice in lexicographic order, consists of 10^6 sweeps of which a small fraction³ is discarded for thermalization. The autocorrelation time $\tau_{\text{int},K}$ has been defined and measured as described in [16].

	exact	local		cluster	
L	K	K	$\tau_{\text{int},K}$	K	$\tau_{\text{int},K}$
8	0.80738	0.8080(5)	5.13(7)	0.80774(32)	1.55(2)
16	0.78914	0.7885(4)	14.4(3)	0.78932(21)	1.90(2)
32	0.77951	0.7795(4)	44.0(1.6)	0.77949(13)	2.29(3)
64	0.77466	0.7742(5)	187(17)	0.77464(8)	2.84(4)
128	0.77223	0.7721(4)	444(58)	0.77221(5)	3.50(5)

Table 2: Monomer density and its integrated autocorrelation time for local and cluster simulations at $m = 0$ and lattice sizes $T = L$.

As one expects for local algorithms we see a steeply rising autocorrelation time hinting at a dynamical exponent not too far from two — we have no ambition here to determine it precisely which would be very costly. One notices, that the error (at fixed sweep number) is almost independent of L . This means the variance just compensates the growing autocorrelation time and decays roughly proportionally to $1/TL$. This is in fact implied by scaling and the canonical dimension of the (connected) 2-point function of the scalar density. Although the integral over the autocorrelation function at $L = 128$ does not look too unconvincing, one may suspect that our number for $\tau_{\text{int},K}$ may only be a lower bound for this case.

The cluster simulations in the last columns consist of 0.6×10^6 sweeps which in our implementation takes about the same time as the local runs on a single PC. We see small slowly rising autocorrelation times. From the two largest lattices one would estimate an effective dynamical exponent $z_{\text{eff}} \approx 0.30$, which is a typical value for cluster algorithms. In total only about 15 CPU hours went into these demonstrations. All codes have been programmed in **MATLAB** and the update routine has about 100 lines (50 without fluctuating boundary conditions).

The cluster algorithm performs very similarly also in the other topological sectors. We did the $T = L = 128$ runs with spin boundary conditions $\varepsilon_\mu = (0, 1)$ (\mathcal{L}_{10}) and found $\tau_{\text{int},K} = 2.68(4)$ and $\varepsilon_\mu = (1, 1)$ (\mathcal{L}_{11}) with $\tau_{\text{int},K} = 2.29(3)$, even shorter than the trivial sector.

³We discard the first $(T/16)^2 \times 1000$ sweeps in the local runs.

The next series of runs to be reported is on $T = L = 128$ lattices at several positive and negative masses. Again each data point is produced by 0.6×10^6 sweeps. These simulations included fluctuating boundary conditions. Recorded observables were the monomer density K , the boundary conditions ε_μ and the topological flags $f_{\alpha\beta}$. From these data the distribution of boundary conditions can be deduced and we checked their correctness. As an example we consider here (3.21) and compute for the right hand side

$$S_{10} = -\frac{2+m}{2} \langle \xi^\top(x) \mathcal{C} \xi(x) \rangle_{10} = \frac{\langle K \rangle - 2 \langle K \delta_{\varepsilon,(1,0)} \rangle}{1 - 2 \langle \delta_{\varepsilon,(1,0)} \rangle}, \quad (5.1)$$

where on the right hand side the Ising ensemble with fluctuating boundary conditions ε is meant. The result at $m = 0$ is $S_{10} = 0.76987(6)$ with the exact value being $0.769800361\dots$ Errors for this combination of observables are estimated as discussed in [16], where the definition of $\tau_{\text{int},S_{10}}$ from the fluctuations relevant for this quantity can be found. We show these autocorrelation times in figure 3. There seems to be a steep rise by about one unit close to $m = 0$. The second plot shows a better resolution of its vicinity. All these numbers stay comfortably small. The combination measured here has no serious sign problem. One could however construct positive cluster estimators for numerator and denominator.

A simple example for the use of an improved estimator exploiting the topological information can be given by the two observables with equal mean

$$\langle \delta_{\varepsilon,(1,0)} \rangle = \left\langle \frac{1}{4} \delta_{(f_{10}, f_{01}, f_{11}), (0,0,0)} + \frac{1}{2} \delta_{(f_{10}, f_{01}, f_{11}), (0,1,0)} \right\rangle. \quad (5.2)$$

The fractions on the right hand are the part of admissible boundary conditions given by $\varepsilon = (1, 0)$. Flag positions not tagged here do not allow this value at all. At $m = 0$ we find in our run for the left hand side $0.18650(66)$ [$\tau_{\text{int}} = 0.852(6)$] and for the other mean $0.18650(37)$ [$\tau_{\text{int}} = 1.38(1)$] while the exact answer is $0.186455866\dots$. Of course, the two estimates are strongly correlated. It is clear that the left estimate is ‘more stochastic’ using the actually picked boundary conditions in the run and τ_{int} is hence smaller. This pattern is typical for cluster estimators with the reduced variance usually overcompensating this effect.

5.2 Four fermion interaction

To simulate the interacting Gross-Neveu model (1.1) we represent each factor Z_ξ^ε in (1.5) by spin-ensembles. Their ε are summed over independently with weights depending on the desired boundary conditions for the fermions. At each site x an overall configuration holds $0 \leq n(x) \leq N$ monomers. The only thing that the

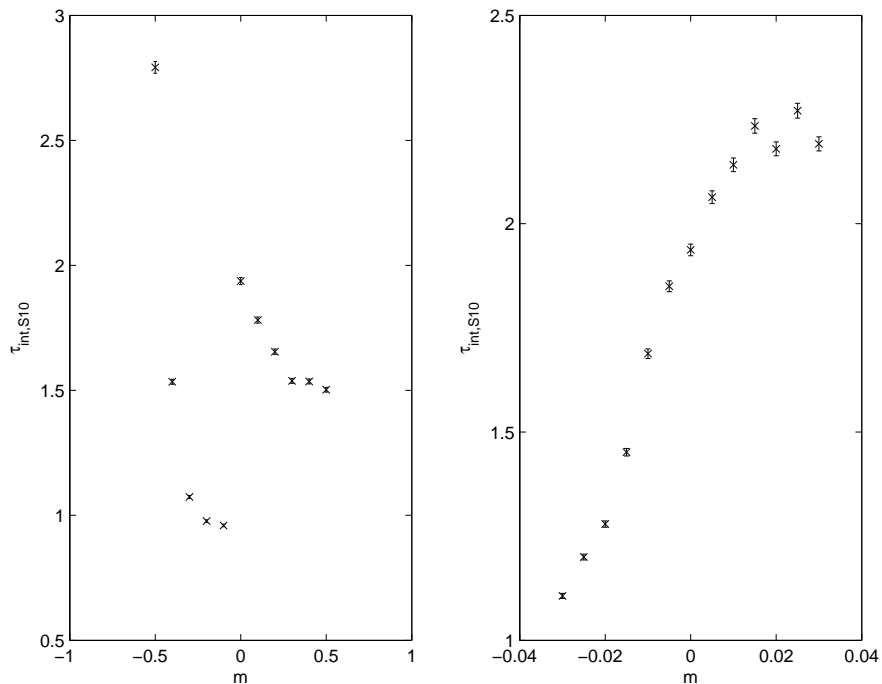


Figure 3: Integrated autocorrelation time for the scalar density (5.1) corresponding to fermion boundary conditions antiperiodic in one direction and periodic in the other at $T = L = 128$.

interaction does is to change the corresponding weight into a factor

$$\exp \left\{ \frac{g^2}{2} \frac{\partial^2}{\partial m^2} \right\} (2+m)^n = \sum_{j=0}^{\lfloor n/2 \rfloor} \frac{n!}{2^j j! (n-2j)!} g^{2j} (2+m)^{n-2j} = c(n, m, g). \quad (5.3)$$

We update one of the spin flavors at a time. Let us introduce the number $\bar{n}(x)$ of monomers in the other momentarily frozen spins. Then in our update the effective monomer weight (or local mass) has to be taken as

$$\varphi|_{\bar{n}(x)} = \frac{c(\bar{n}(x) + 1, m, g)}{c(\bar{n}(x), m, g)}. \quad (5.4)$$

The first few terms are

$$\varphi|_0 = 2+m, \quad \varphi|_1 = 2+m + \frac{g^2}{2+m}, \quad \varphi|_2 = 2+m + 2g^2 \frac{2+m}{(2+m)+g^2}, \dots \quad (5.5)$$

In interacting theories the mass of Wilson fermions undergoes additive renormalization. Both in the Thirring model ($N = 2$) and in the higher N Gross-Neveu

model perturbative and nonperturbative calculations [4] as well as large N approximations yield negative values for the critical mass $m_c(g^2)$ close to which one wants to simulate. This is why it was crucial to extend the cluster algorithm to also accommodate $\varphi < 2$.

5.3 Additional gauge coupling

An amusing exercise is to add to the Majorana ‘flavor’ group a ‘color’ $Z(2)$ gauge interaction. We describe it here only very briefly. We now make use of the gauge links in (2.1) and consider

$$Z_{\text{color}} = \sum_{\tau(x,\mu)} e^{\beta \sum_p \tau_p} (Z_s^\varepsilon[m, \tau])^N \quad (5.6)$$

with the plaquette field τ_p made from the links $\tau(x, \mu) = \pm 1$. The self-interaction can always be added, changing only the monomer weights. We suppress it here. Each dimer loop receives as an additional factor the Wilson loop made of τ . By Stokes’ theorem they can be replaced by a product of τ_p either on all plaquettes where a + spin resides or on those where the negative spins sit, see figure 1. Let us choose +. In the case of antiperiodic boundary conditions additional loops around the torus appear where the torus closes (where the clamps were). As a two-dimensional gauge theory is rather trivial the τ sum can be carried out. We need to know how many plaquettes get tiled with τ_p an odd number of times. Let us introduce the ‘composite’ flavor spin-field

$$S(\underline{x}) = s^{(1)}(\underline{x})s^{(2)}(\underline{x}) \cdots s^{(N)}(\underline{x}). \quad (5.7)$$

Then

$$M_\pm = \sum_{\underline{x}} \delta_{S(\underline{x}), \pm} \quad (5.8)$$

contain this information and the extra weight from summing over τ is

$$2^{2TV} [\cosh(\beta)^{M_+} \sinh(\beta)^{M_-} + \cosh(\beta)^{M_-} \sinh(\beta)^{M_+}].$$

This is equivalent to a magnetic field

$$H = -\frac{1}{2} \ln \tanh(\beta) \quad (5.9)$$

coupled to S and fluctuating in sign. In addition we only get contributions if an even number of flavors is antiperiodic in each direction separately (due to $Z(2)$ confinement). The fluctuating magnetic field can presumably be included in the cluster simulation without problems. As we update a given flavor, each spin can in addition bond to one exterior (‘phantom’) spin.

6 Conclusion and Outlook

It seems that with the new cluster algorithm the Gross-Neveu model (and the Thirring model) are wide open for high precision simulation. Further observables, in particular cluster estimators, remain to be constructed. The $O(N)$ Noether currents may be accessible, for example. Also ratios of partition functions like Z_s^{00}/Z_s^{10} etc. are expected to have a continuum limit and may serve as renormalized finite volume couplings. Majorana fermions are prominent in supersymmetry. Maybe some studies on two dimensional supersymmetry become possible with simulations very close to the continuum limit.

An obvious question that every reader will have is if any of this carries over to higher dimension and/or more complicated gauge interactions. Let us first caution here: fermions in one space dimension are very special. This has manifested itself in other so-called Fermi-Bose equivalences in two dimensions. At the heart of this in operator language is the fact that the Jordan-Wigner [17] transformation transforms anticommuting to commuting degrees of freedom *without* generating non-localities. This has no obvious generalization to higher dimension (see however [18]). The fact that we find positive weights for all topologically trivial loops in a way seems to be the euclidean counterpart. Also that Majorana fermions are in some sense equivalent to Ising spins it not new, of course, see [19], [20]. The main achievement here is that we simulate in a standard (lattice) euclidean fermion formulation and can get really critical. In higher dimension a dimer representation for fermions can probably be constructed along similar lines, but the weight will be sign-fluctuating in a more essential fashion. The slight hope may be that one could be able to handle this sign problem with cluster estimators. In addition, the coupling to gauge fields contributing fluctuating Wilson loops is an open problem. There are ongoing efforts to simulate discrete models dual to nonabelian gauge theories (spin foam) (see [21] and references therein). This may be an interesting view on gauge theories in the context of the approach to fermions developed here. In any case, the goal is attractive enough to warrant further thought.

We would like to acknowledge discussions about the Gross-Neveu model on the lattice with Francesco Knechtli, Björn Leder, Rainer Sommer and most of all Tomasz Korzec. We also thank the Deutsche Forschungsgemeinschaft (DFG) for support in the framework of SFB Transregio 9.

A Exact Majorana partition functions

The Pfaffian is defined for an antisymmetric matrix A_{ij} of even size, $i, j = 1, \dots, 2n$,

$$\text{Pf}(A) = \int d^{2n} \xi e^{-\frac{1}{2} \xi^\top A \xi} = \frac{1}{2^n} \frac{1}{n!} \epsilon_{i_1 i_2 \dots i_{2n}} A_{i_1 i_2} A_{i_3 i_4} \dots A_{i_{2n-1} i_{2n}}, \quad (\text{A.1})$$

where we integrate over $2n$ Grassmann variables and a sign convention for the measure is implied. By a change of variables $\xi \rightarrow F\xi$ one sees the well known identity

$$\text{Pf}(F^\top AF) = \det(F) \text{Pf}(A), \quad (\text{A.2})$$

and by squaring the integral in (A.1),

$$[\text{Pf}(A)]^2 = \det(A) \quad (\text{A.3})$$

follows.

We are interested in $A = \mathcal{C}(\gamma_\mu \tilde{\partial}_\mu + m - \frac{1}{2} \partial^* \partial)$ with boundary conditions ε . The determinant immediately follows by Fourier diagonalization

$$\det_\varepsilon(A) = \prod_p (\hat{p}^2 + M(p)^2) \quad (\text{A.4})$$

with

$$p = \left(\frac{2\pi}{T}(n_0 + \varepsilon_0/2), \frac{2\pi}{L}(n_1 + \varepsilon_1/2) \right), \quad n_0 = 0, \dots, T-1, \quad n_1 = 0, \dots, L-1 \quad (\text{A.5})$$

and

$$\hat{p}_\mu = \sin(p_\mu), \quad M(p) = m + \frac{1}{2} \hat{p}^2, \quad \hat{p}_\mu = 2 \sin(p_\mu/2). \quad (\text{A.6})$$

In this article we also want to know the relative signs of $\text{Pf}(A)$ for different boundary conditions and possibly negative m . This information is lost in the determinant and we proceed differently.

We define the unitary Fourier transformation matrix

$$F_{xp} = \frac{1}{\sqrt{TL}} e^{ipx} \quad (\text{A.7})$$

which is augmented trivially to include a unit matrix in spin space. Then, using (A.2) we get

$$\det(F) \text{Pf}(A) = \text{Pf}(\tilde{A}) \quad (\text{A.8})$$

with

$$\tilde{A}_{qp} = \mathcal{C}(\gamma_\mu \hat{p}_\mu + M(p)) \delta_{p+q,0}. \quad (\text{A.9})$$

The factor $\det(F)$ is just a phase that we fix later.

The matrix \tilde{A} consists of antisymmetric blocks where momenta $p, -p$ get paired. If they are different (modulo 2π) such a block contributes *one* factor $(\hat{p}^2 + M(p)^2)$ to the Pfaffian.

For simplicity we now restrict our discussion to both T and L even. Then all momenta get paired non-trivially except $p = (0, 0), (\pi, 0), (0, \pi), (\pi, \pi)$ in the all periodic case $\varepsilon_\mu = (0, 0)$. We may summarize this result by

$$\text{Pf}_\varepsilon(A) = \prod_p \sqrt{\dot{p}^2 + M(p)^2} \times \begin{cases} \text{sign}[m(m+4)] & \text{for } \varepsilon_\mu = (0, 0) \\ 1 & \text{other } \varepsilon_\mu \end{cases}. \quad (\text{A.10})$$

Possible extra phase factors can be excluded by considering the limit $m \rightarrow \infty$. Note that the double periodic Pfaffian changes sign at $m = 0$.

In this article we need for comparison the scalar condensate in ensembles that in fermion language have the partition function

$$\bar{Z}_\xi[m] = \sum_\varepsilon c(\varepsilon) Z_\xi^\varepsilon[m]. \quad (\text{A.11})$$

It is given by

$$-\frac{1}{2} \langle \xi^\top \mathcal{C} \xi \rangle_c = \frac{1}{TL} \frac{\partial}{\partial m} \ln(\bar{Z}_\xi) = -\frac{1}{2} \frac{\sum_\varepsilon c(\varepsilon) z(\varepsilon, m) \langle \xi^\top \mathcal{C} \xi \rangle_\varepsilon}{\sum_\varepsilon c(\varepsilon) z(\varepsilon, m)} \quad (\text{A.12})$$

with

$$z(\varepsilon, m) = \frac{Z_\xi^\varepsilon[m]}{\sum_{\varepsilon'} Z_\xi^{\varepsilon'}[m]} \quad (\text{A.13})$$

and

$$-\frac{1}{2} \langle \xi^\top \mathcal{C} \xi \rangle_\varepsilon = \frac{1}{TL} \sum_p \frac{M(p)}{\dot{p}^2 + M^2(p)}. \quad (\text{A.14})$$

All these exact results can be easily evaluated for any finite lattice that is simulated. For $\varepsilon_\mu = (0, 0), m \rightarrow 0$ the product $z \langle \xi^\top \mathcal{C} \xi \rangle_{(0,0)}$ remains finite but requires precaution numerically.

The continuum limit of z can presumably be computed analytically. We here content ourselves with the numerical construction of their Symanzik expansion in a few cases. We set $T = L$ (aspect ratio one) and

$$z(\varepsilon, m)|_{mL=\kappa} \simeq \sum_{k \geq 0} d_k(\kappa, \varepsilon) L^{-k} \quad (\text{A.15})$$

and compile some values in table 3.

The analysis of the asymptotic series was carried out as described in appendix D in [22]. The ε missing in the table can be computed from those given. Digits are quoted such that there is at most an uncertainty of one in the last digit. For $\kappa = 0$ odd corrections vanish.

κ	ε	d_0	d_2	d_4
0	(1,0)	0.3135575596	-0.219897	-1.1
κ		d_0	d_1	d_2
1	(0,0)	0.12681663	-0.048092	-0.108
1	(1,0)	0.27632955	0.012935	-0.135
-1	(0,0)	-0.16991195	-0.08631	0.183
-1	(1,0)	0.37023294	0.030368	-0.285

Table 3: Symanzik expansion coefficients for ratios of partition functions at different boundary conditions in the finite volume continuum limit at fixed $\kappa = mL$.

References

- [1] C. Gattringer, Nucl. Phys. B543 (1999) 533, hep-lat/9811014.
- [2] C. Gattringer, V. Hermann and M. Limmer, (2007), arXiv:0704.2277 [hep-lat].
- [3] D.J. Gross and A. Neveu, Phys. Rev. D10 (1974) 3235.
- [4] T. Korzec and U. Wolff, PoS LAT2006 (2006) 218, hep-lat/0609022.
- [5] W.E. Thirring, Annals Phys. 3 (1958) 91.
- [6] S.R. Coleman, Phys. Rev. D11 (1975) 2088.
- [7] P. Rossi and U. Wolff, Nucl. Phys. B248 (1984) 105.
- [8] I.O. Stamatescu, Phys. Rev. D25 (1982) 1130.
- [9] F.J. Wegner, J. Math. Phys. 12 (1971) 2259.
- [10] R.H. Swendsen and J.S. Wang, Phys. Rev. Lett. 58 (1987) 86.
- [11] U. Wolff, Phys. Rev. Lett. 62 (1989) 361.
- [12] M. Hasenbusch, J. Phys. (Paris) I 3 (1993) 753, hep-lat/9209016.
- [13] J. Hoshen and R. Kopelman, Phys. Rev. B 14 (1976) 3438.
- [14] R.C. Brower and S. Huang, Phys. Rev. D41 (1990) 708.
- [15] B. Bunk, Fermion Algorithms, Jülich, 1991, World Scientific.
- [16] ALPHA, U. Wolff, Comput. Phys. Commun. 156 (2004) 143, hep-lat/0306017.

- [17] P. Jordan and E.P. Wigner, *Zeit. Phys.* 47 (1928) 631.
- [18] E.H. Fradkin, M. Srednicki and L. Susskind, *Phys. Rev. D* 21 (1980) 2885.
- [19] T.D. Schultz, D.C. Mattis and E.H. Lieb, *Rev. Mod. Phys.* 36 (1964) 856.
- [20] J.B. Kogut, *Rev. Mod. Phys.* 51 (1979) 659.
- [21] J.W. Cherrington, D. Christensen and I. Khavkine, (2007), arXiv:0705.2629 [hep-lat].
- [22] ALPHA, A. Bode, P. Weisz and U. Wolff, *Nucl. Phys. B* 576 (2000) 517, hep-lat/9911018.